

IMPACT OF THREE DIFFERENT DOUBLE BAFFLE DESIGNS ON THE THERMAL PERFORMANCE OF SQUARE DUCTS

Amnart Boonloi^a and Withada Jedsadaratanachai^{b,*}

^a Department of Mechanical Engineering Technology, College of Industrial Technology, King Mongkut's University of Technology North Bangkok, Bangkok 10800, Thailand

^b Department of Mechanical Engineering, School of Engineering, King Mongkut's Institute of Technology Ladkrabang, Bangkok 10520, Thailand

ABSTRACT

CFD analyses of flow characteristics and heat transfer topology in a heat exchanger duct (HXD) placed with three various configurations of the double V-baffles (DVB) are reported. Parameters of interest are DVB height ratios ($b/H = 0.05 - 0.25$), gap spacing ratios ($g = 0.05 - 0.40$), flow directions (+x, -x), and DVB configurations (Type I, II and III). Laminar flow with Reynolds numbers (based on the inlet conditions) between 100 – 2000 is measured. The present problem is solved with the finite volume method (a commercial program). Fluid flow and heat transfer characteristics in the tested duct are described. Thermal assessments of the tested duct are also presented. Simulation results showed that the installation of the DVB in the HXD results in higher heat transfer rate due to the creation of the vortex flow and the disturbance of the thermal boundary layer (TBL). Different flow structures and heat transfer behavior are observed when gap spacing ratios, flow directions and DVB shapes are changed. In addition, the type II DVB provides the highest TEF of 3.55 at $b/H = 0.10$, $g/H = 0.25$ for the -x flow direction.

Keywords: double V-baffles; heat transfer; thermal performance; flow structures; heat exchanger.

1. INTRODUCTION

Baffles, rib, winglets, wings, etc., are called “vortex generators or turbulators” (Boonloi and Jedsadaratanachai (2020), Boonloi and Jedsadaratanachai (2021b)). An installation of these vortex generators is a passive method to improve heat-exchanger performance. The vortex generators produce vortex flows in heat exchangers that cause TBL to be disturbed. The disturbed TBL is an important reason for an increase in heat transfer coefficients. The vortex-generator developments have been done with various objectives such as to increase thermal performance, to improve vortex-generator stabilization, to ease installation and maintenance, etc.

In this paper, some research about the vortex - generator development can be summarized as follows. Experimental and numerical investigations of a rectangular channel placed with perforated baffles were presented by Habet *et al.* (2021). The baffles were placed on the upper-lower channel walls in in-line and staggered arrangements. They found that the staggered arrangement performs higher thermal enhancement factors than the in-line arrangement. Faujdar and Agrawal (2021) numerically studied thermal performance development of a solar air heater (SAH) duct installed with perforated V-down baffles underneath an absorber plate. Sharma *et al.* (2022) improved the thermal performance of a solar thermal collector with discrete V-down baffles. They reported that the CFD analysis helps to explain flow and heat transfer topologies of the experiment. Chang *et al.* (2019) enhanced the heat transfer rate of a square channel by inclined baffles and perforated slots. They presented that the averaged Nusselt number is 5 – 9 times higher than the general plain duct, while the thermal performance factor is 1.6 – 3.2 and 2 – 3.4, respectively, for forward and backward flows. The effects of longitudinal baffles in a spiral SAH were presented by Jia *et al.* (2021). Sahin *et al.* (2019) proposed the optimal design of hollow trapezoidal baffles in a heat sink. Six parameters (i.e., the corner angle

(α), the inclination angle (β), the baffle height (H), the baffle length (L), the baffle width (S) and Reynolds number) were measured. They reported that the maximum heat transfer rate is detected in the case of $Re = 17,000$, $H = 36$ mm, $L = 45$ mm, $S = 26$ mm $\alpha = 0^\circ$, $\beta = 0^\circ$, while the minimum friction loss is obtained in the case of $Re = 17,000$, $H = 20$ mm, $L = 25$ mm, $S = 26$ mm, $\alpha = 16^\circ$, $\beta = 0^\circ$. Lori and Vafai (2022) numerically analyzed the fluid flow and heat transfer of a microchannel heat sink installed with periodic vertical porous ribs. Effects of various geometrical shapes including rectangular, elliptical, isosceles triangular, backward triangular and forward triangular on the walls of the microchannel on thermal performance were compared. They found that the average Nusselt number of the microchannel with the porous ribs is 1.30 – 2.16 and 2.505 – 4.01 times greater than the solid rib and no rib, respectively. Muñoz-Cámara *et al.* (2019) experimentally observed the thermo-hydraulic performance and heat transfer profiles in circular-orifice baffled tubes. An experimental investigation on thermal performance of a SAH duct installed with apex-up discrete arc ribs was reported by Bhuvad *et al.* (2021). They observed that the best heat transfer rate is around 2.92 times greater than the general SAH duct. Gill *et al.* (2021) studied the optimal parameters of a SAH duct roughened with hybrid ribs. They found that the proposed design yields the heat transfer rate around 3.16 times higher when compared with the smooth duct. Du and Hong (2021) numerically analyzed the influences of inward sinusoidal ribs in a tube heat exchanger for waste heat recovery. They concluded that the highest performance is around 1.73. Aerothermal performance of a square duct inserted with inclined ribs and slots was performed by Change *et al.* (2021). They concluded that the inclined ribs and slots provides the averaged Nusselt number of 4.2 – 3.8 times higher than that of the smooth duct. Numerical simulations of flow and heat transfer for a channel placed with multi V-shaped baffles was reported by Li *et al.* (2018). Azad *et al.* (2021) reported the numerical and experimental investigations on SAH performance with discrete arc ribs.

* Corresponding author. Email: withada.je@kmitl.ac.th

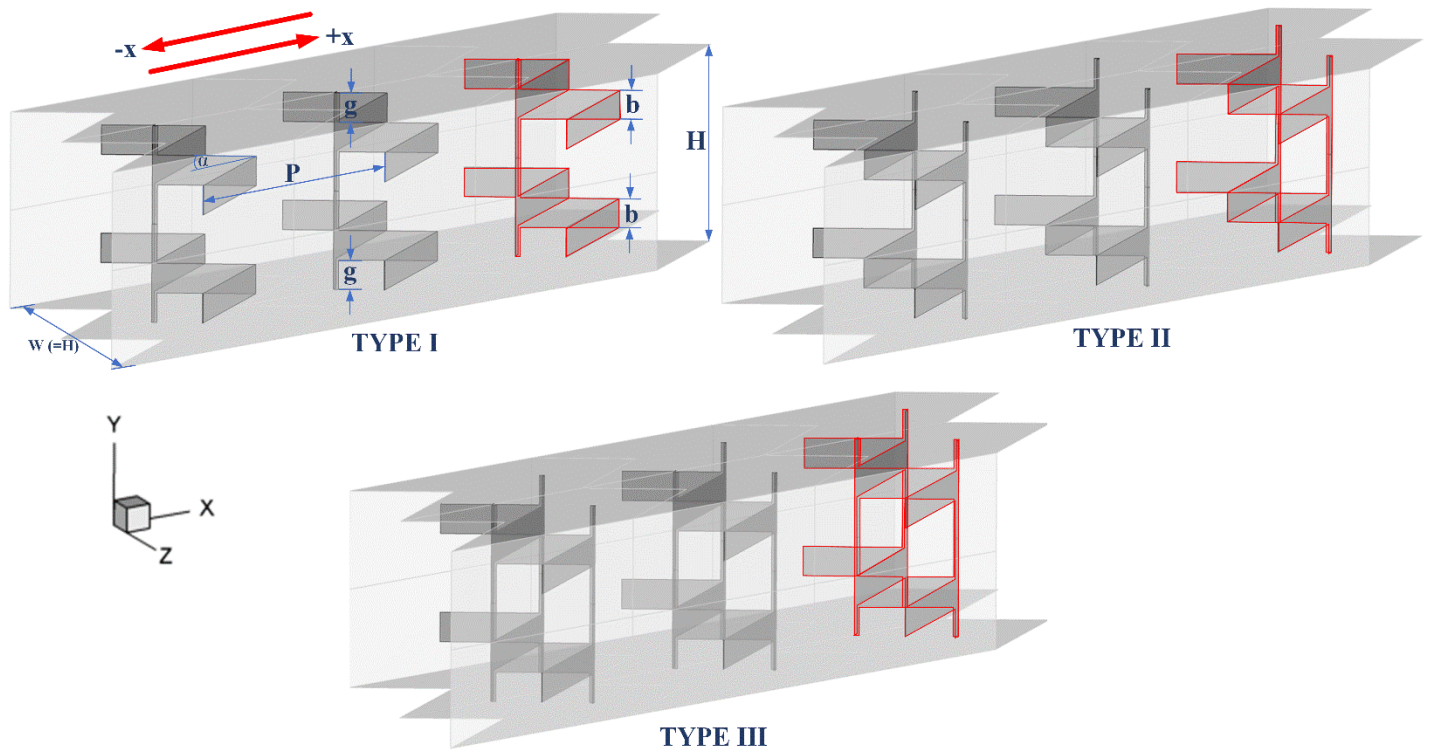


Fig. 1 HXD inserted with three configurations of the DVB.

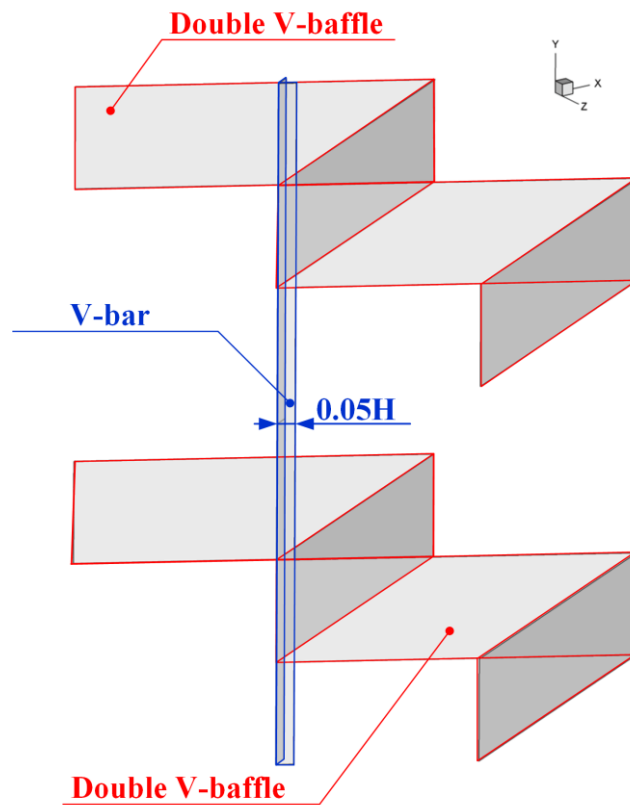


Fig. 2 DVB configuration.

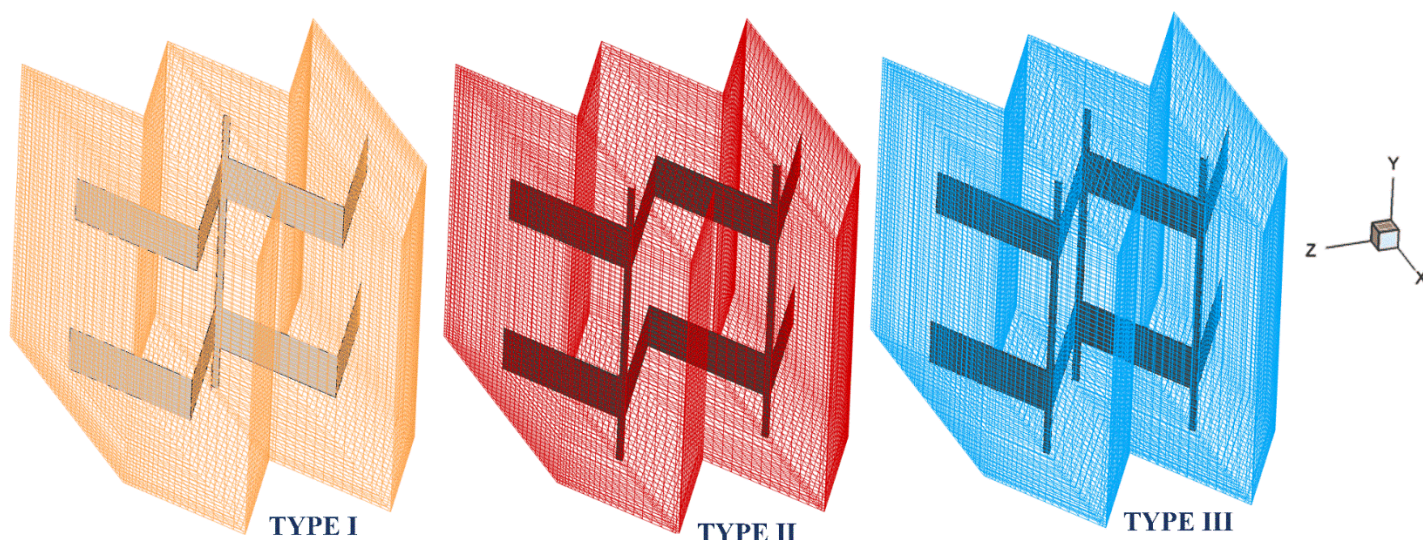


Fig. 3 Mesh elements of the numerical models.

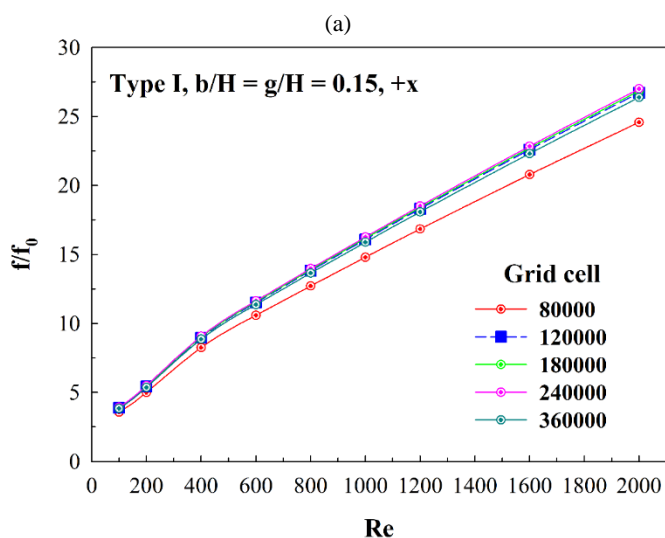
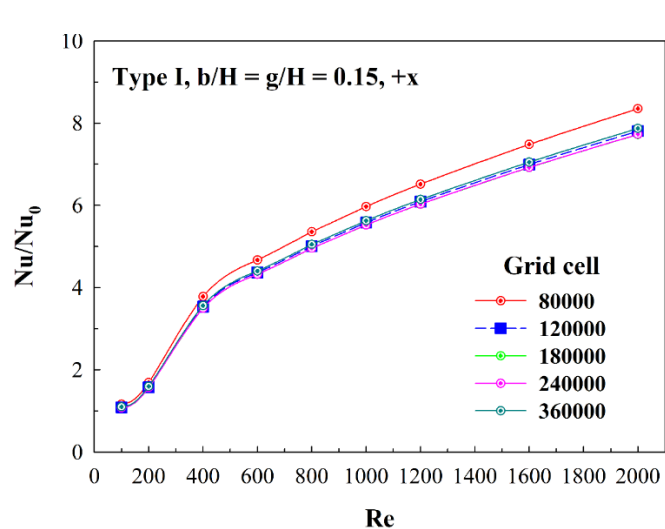


Fig. 4 Grid independence for (a) Nu/Nu_0 and (b) f/f_0 .

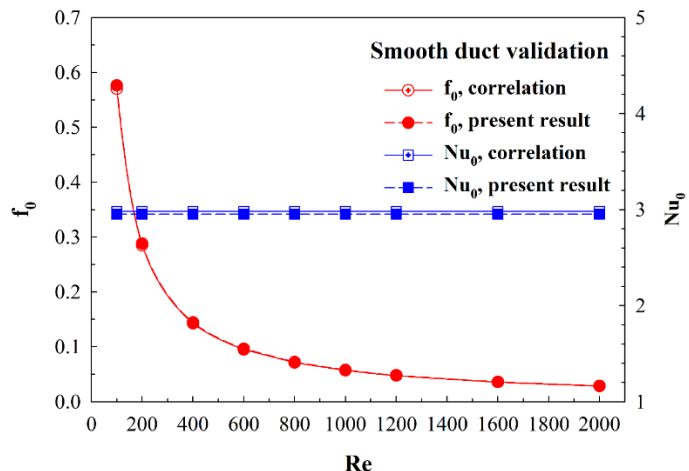


Fig. 5 Smooth duct validation.

The variation of rib elements was considered for Reynolds number in a range of 3000 – 14,000. They summarized that the best heat transfer rate is around 3.88 times greater the general plain duct. Kumar *et al.* (2021) improved the SAH performance with polygonal and trapezoidal ribs. They found that the best SAH performance of their investigated range is around 1.89. Moreover, Boonloi and Jedsadaratanachai (2021a) and Jedsadaratanachai and Boonloi (2014) improved the heat exchanger performance with double V-shaped vortex generators. They found that the double V-shaped vortex generators provided high effectiveness to improve heat-exchanger performance.

In the present research, the vortex generators are developed with the two main aims: 1. to increase the number of vortex cores that improve fluid-temperature distribution and 2. to improve the stabilization of the vortex - generator structure. To increase the number of the vortex cores, the double V-baffle (DVB) with gap spacing is selected to produce the vortex flows. The V-shaped bar or V-bar is added to the DVB to enhance the stabilization of the vortex-generator structure. The V-bar can also increase the vortex core number and improve the fluid turbulent mixing in the heat exchanger duct (HXD). The DVB can be separated into three types. The DVB with one, two and three V-bars are called Type I, Type II and Type III, respectively. Effects of DVB heights, gap spacings (or local in transverse plane) and flow directions on fluid streamlines and heat transfer topologies are studied numerically for the Reynolds number within 100 – 2000 (laminar flow considering at the inlet condition). The understanding of flow and heat transfer mechanisms is a critical knowledge for the thermal improvement of the heat exchangers.

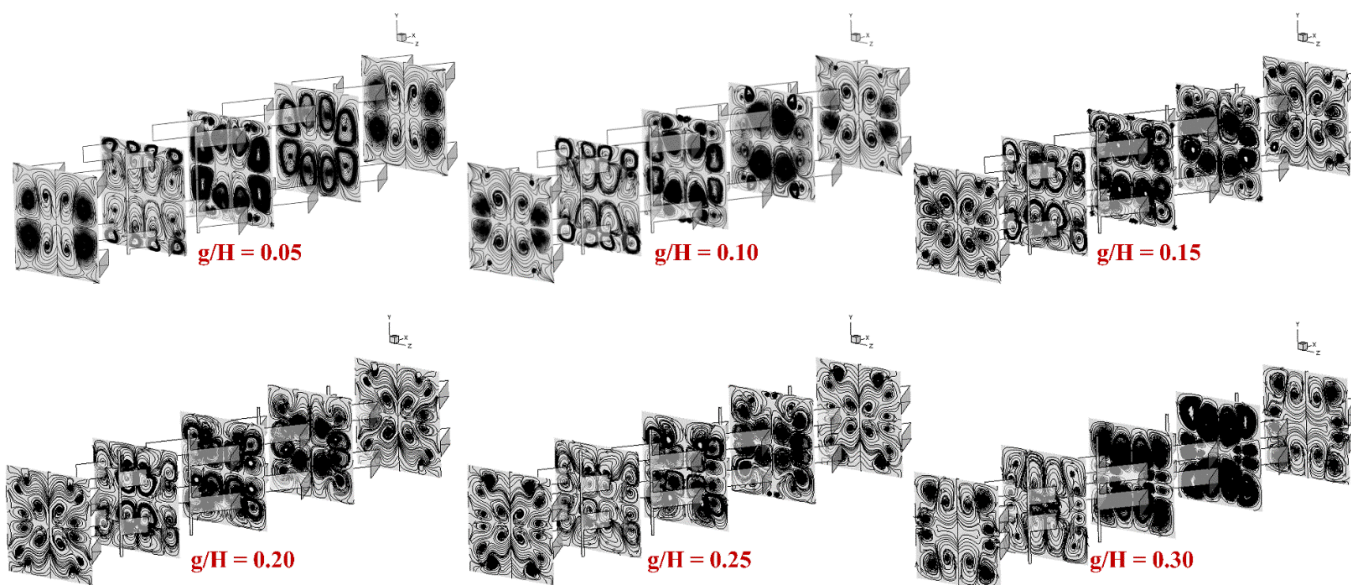


Fig. 6 Streamlines in transverse planes of the HXD inserted with the type I DVb at various g/H for $b/H = 0.15$, $+x$ and $Re = 600$.

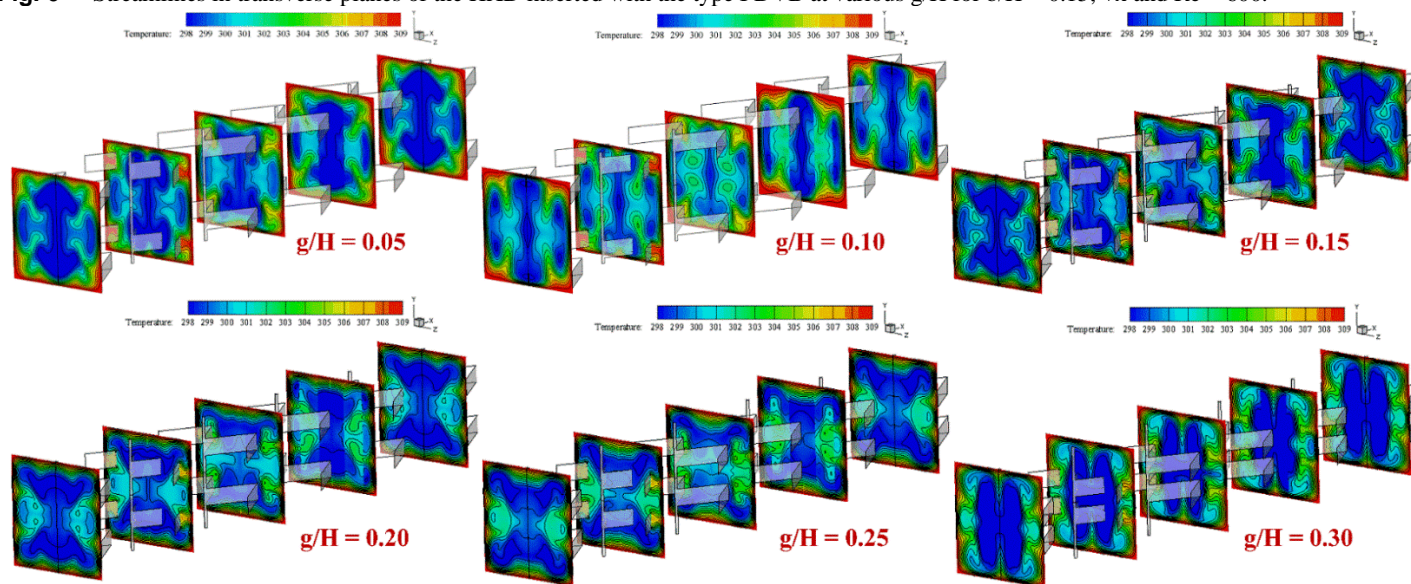


Fig. 7 Temperature distributions in transverse planes of the HXD inserted with the type I DVb at various g/H for $b/H = 0.15$, $+x$ and $Re = 600$.

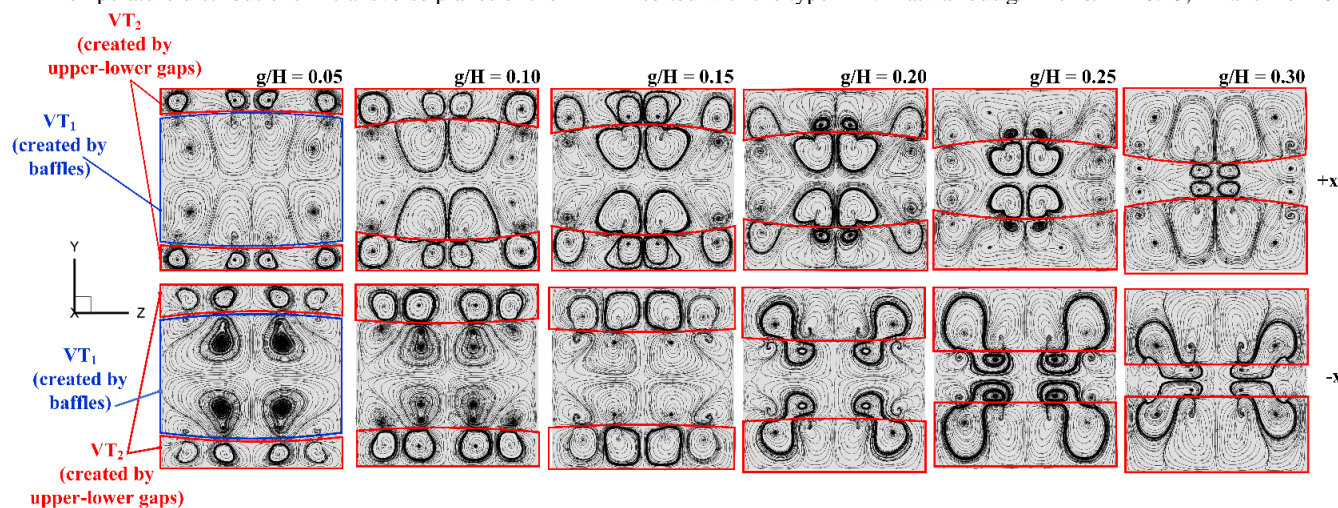


Fig. 8 Flow patterns of the HXD inserted with the type I DVb at various g/H and flow directions for $b/H = 0.15$ and $Re = 600$.

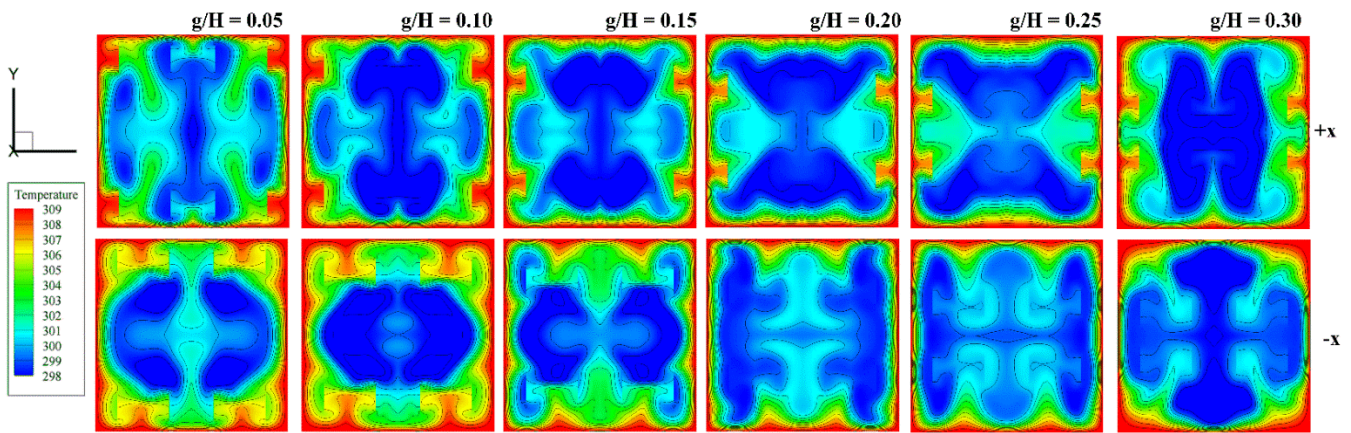


Fig. 9 Temperature distributions in transverse planes of the HXD inserted with the type I DVB at various g/H and flow directions for $b/H = 0.15$ and $Re = 600$.

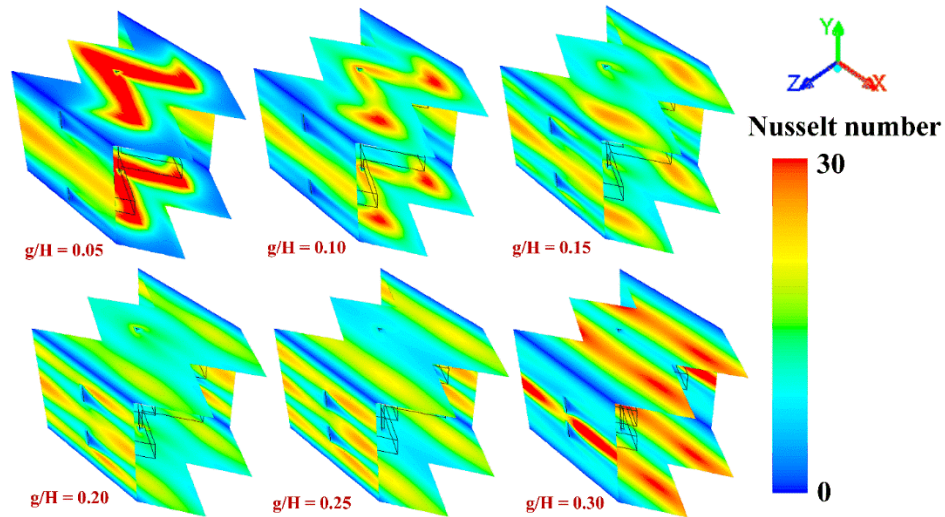


Fig. 10 Local Nusselt number contours of the HXD inserted with the type I DVB at various g/H for $b/H = 0.15$, $+x$ and $Re = 600$.

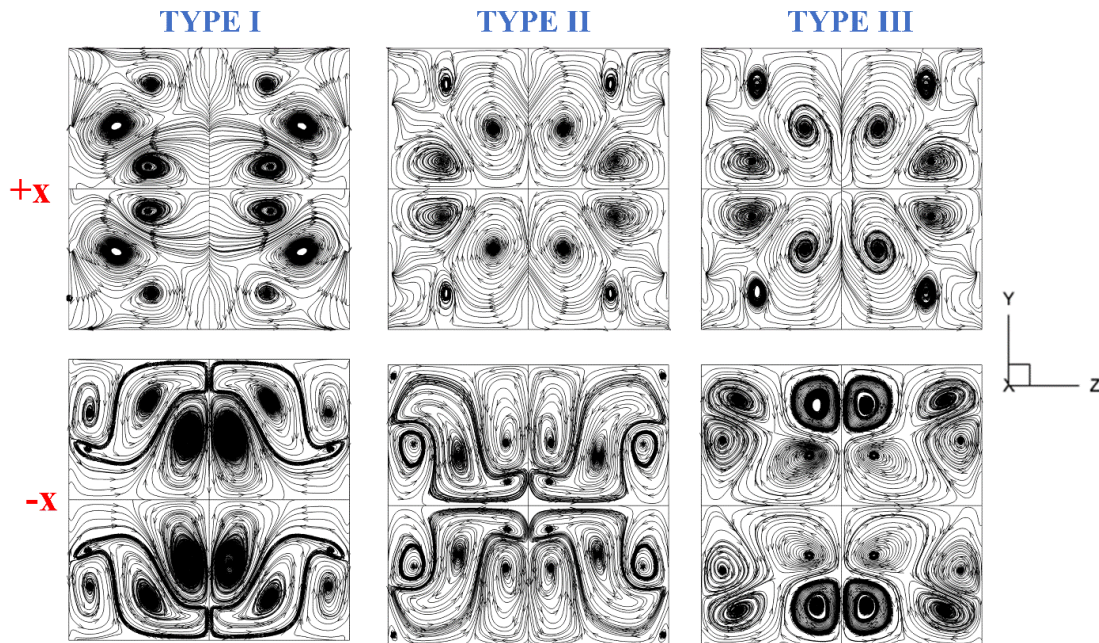


Fig. 11 Streamlines in transverse planes of the DVB inserted with various DVB types and flow directions for $b/H = 0.20$, $g/H = 0.10$ and $Re = 800$.

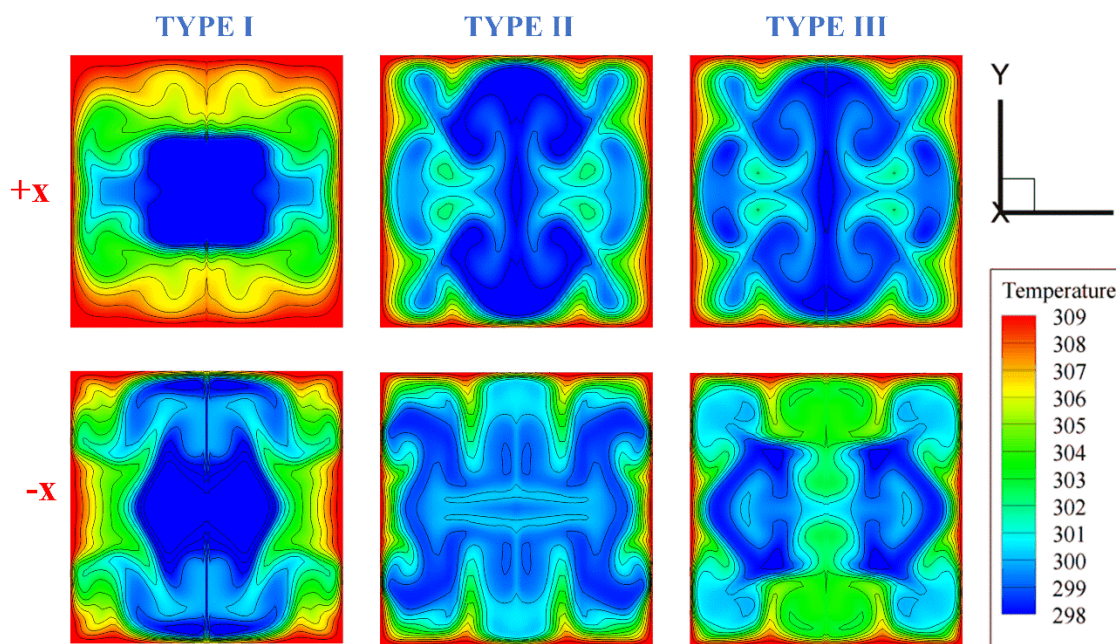


Fig. 12 Temperature distributions in transverse planes of the HXD inserted with various DVB types and flow directions for $b/H = 0.20$, $g/H = 0.10$ and $Re = 800$.

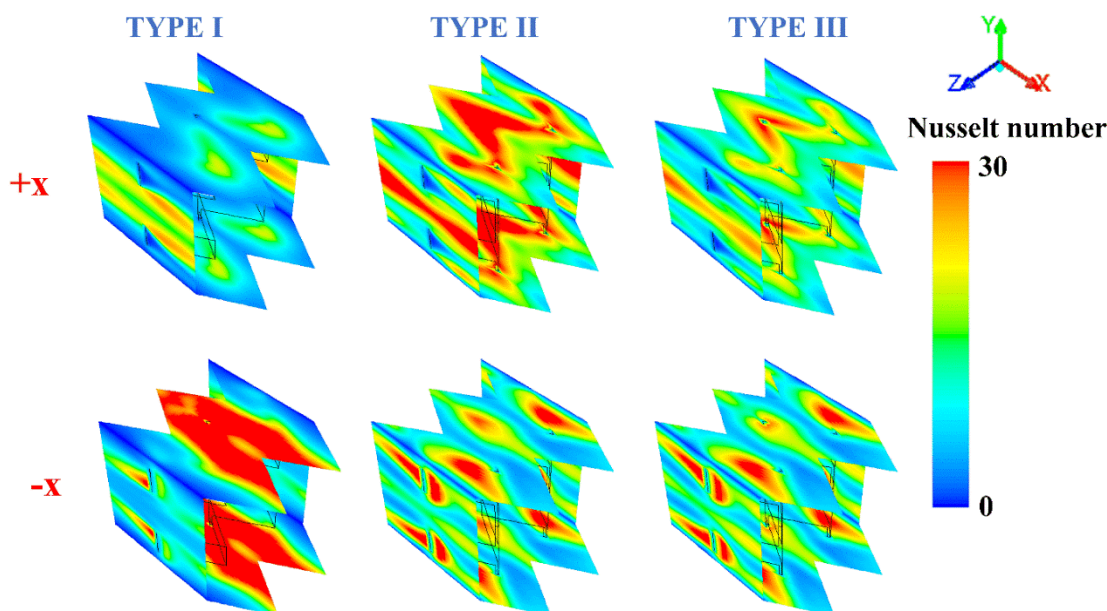


Fig. 13 Local Nusselt number contours of the HXD inserted with various DVB types and flow directions for $b/H = 0.20$, $g/H = 0.10$ and $Re = 800$.

2. SIMULATED MODEL

Fig. 1 reports the simulated models of the HXD installed with three kinds of the DVB. Type I is the DVB with one V-bar (see Fig. 2), while Type I and III are the DVB with two and three V-bars, respectively. The HXD hydraulic diameter, D_h , is equivalent to 0.05 m. The HXD height, H , is equal to the HXD hydraulic diameter. The DVB height is represented by “ b ”. The DVB height to the HXD height, b/H , is adjusted within the range of 0.05 – 0.25. The gap distance or gap spacing between the upper/lower edge of the DVB and the upper/lower HXD wall is represented by “ g ”. The gap spacing to the HXD height, g/H , is varied within the range of 0.05 – 0.40 which is subject to the baffle height. The flow attack angle of 30° is selected for all investigated cases. The distance between the DVBS, P , is identical to HXD height, $P = H$. The V-bar thickness is equal to $0.05H$. Two flow directions, $+x$ and $-x$, are considered. The Reynolds

number within the range around 100 – 2000 is investigated. The periodic modules of the HXD equipped with the DVB are illustrated in Fig. 3.

3. MATHEMATICAL FOUNDATION, BOUNDARY AND INITIAL CONDITIONS

The present numerical method is referred from Ref. (Boonloi and Jedsadaratanachai (2021a) and Jedsadaratanachai and Boonloi (2014)). The fluid flow and heat transfer in the tested duct are considered to be steady in three dimensions. The working fluid in the HXD is air at the initial temperature of 300 K with the Prandtl number of 0.707. Because the air velocity within the investigated range is very low, fluid is considered to be incompressible. The fluid properties within the tested range are considered as constant values at the average temperature because of the maximum temperature difference is not higher than 10°C . Body force and viscous dissipation are ignored. For the heat transfer

mode, forced convection is considered, while natural convection and radiation are disregarded. The no-slip condition is set for all HXD surfaces. The air velocity at the inlet condition of the HXD equipped with the DVB is stated in terms of Reynolds number. The Reynolds number can be calculated by Eq. 1.

$$Re = \frac{\rho \bar{u} D_h}{\mu} \quad (1)$$

The pressure loss within the HXD equipped with the DVB is represented by friction factor, which can be determined by Eq. 2.

$$f = \frac{(\Delta p / L) D_h}{1/2 \rho \bar{u}^2} \quad (2)$$

The heat transfer rate in the tested duct can be concluded as local Nusselt number (Nu_x) and average Nusselt number (Nu), which are written as in Eq. 3 and 4, respectively.

$$Nu_x = \frac{h_x D_h}{k} \quad (3)$$

$$Nu = \frac{1}{A} \int Nu_x dA \quad (4)$$

The benefit of the DVB installation can be considered by the increments of heat transfer rate at an identical pumping power, which is known as thermal enhancement factor (TEF). The TEF can be calculated by Eq. 5.

$$TEF = \frac{h}{h_{0,pp}} = \frac{Nu}{Nu_{0,pp}} = (Nu / Nu_0) / (f / f_0)^{1/3} \quad (5)$$

The boundary conditions of the present numerical model are summarized in Table 1.

Table 1 Boundary conditions of the HXD equipped with the DVB.

| Zone | Boundary condition |
|---------------------------|------------------------------|
| Entrance and exit regimes | Periodic boundary |
| HXD walls | Uniform temperature of 310 K |
| DVB and V-bar surfaces | Insulator |

4. NUNERUCAL VALIDATION

For the simulation, the numerical validation of the simulated model is an important step which helps to increase the credibility of the numerical results. In this work, the numerical validation can be separated into two steps; 1. grid independence or optimum grid check (see Fig. 4) and 2. smooth duct validation (see Fig. 5). For the grid independence, the simulated models of the tested duct ($b/H = g/H = 0.15$, type I, the +x flow direction) with different grid elements (80000, 120000, 180000, 240000 and 360000) are evaluated. The results reveal that the Nusselt number and the friction factor are in similar trend with the deviations around $\pm 2.5\%$ for the grid cells around 120000 – 360000. Considering the computational time and computer resource, the grid cell around 120000 is selected for all simulated models.

For the smooth duct validation, the comparison between the present prediction and the correlations values (Cengel and Ghajar (2015)) for both Nusselt number and friction factor are performed. The results show that the Nusselt number differs from the correlation value within $\pm 0.95\%$ and $\pm 1.2\%$ for the friction factor. Thus, the simulated model has reliability to study flow and heat transfer topologies of the HXD inserted with the DVB.

5. NUMERICAL RESULTS

There are two major topics for consideration; 1. the reports of flow topologies and heat transfer patterns and 2. the assessments of HXD performance. The plots of streamlines in cross-sectional planes, temperature distribution in transverse planes and the local Nusselt number on the HXD walls at various parameters are presented in the first part. The relation graphs of the Nu/Nu_0 , f/f_0 and TEF within the HXD equipped with the DVB are reported in the second part.

5.1 Flow and heat transfer in the HXD equipped with the DVB

Figs. 6 and 7 plots the streamlines in transverse planes and the temperature distributions in transverse planes of the HXD with various

g/H values for the type I DVB, $b/H = 0.15$, $Re = 600$ and the +x flow direction, respectively. As shown in the figure, the results of the DVB installation are 1. the creation of the vortex flows, 2. the better fluid blending and 3. the TBL disturbance. These three behaviors lead to an increase in the heat transfer rate. The vortex flows close to the duct walls which contribute to the TBL disturbance, while the vortex streams at the core of the test duct assist fluid mixing or fluid temperature distributions. There are around 4 – 16 vortex centers through the tested duct. The number of vortices directly impacts the fluid temperature distributions.

Fig. 8 presents the changes of the vortex flows in the test duct when the g/H ratios for both flow directions are varied. The vortex flows can be divided into two parts: 1. the vortex streams which are introduced by the DVB called “VT₁” and 2. the vortex streams which are formed by the upper-lower gaps called “VT₂”. The VT₁ is found at the center of the HXD, while the VT₂ is observed at the upper-lower edges of the tested duct. In almost cases, the VT₁ improves the fluid mixing, while the VT₂ leads to the TBL disturbance on the heat transfer surface. These two behaviors are key behaviors that lead to the enhancement of heat transfer rates and thermal performance. When the g/H ratio increases, the VT₂ expands but the VT₁ constricts for both flow directions.

Fig. 9 reports the variations of the fluid-temperature distributions in transverse planes when the g/H ratio for both flow directions are varied. It is clearly seen that g/H ratios and flow directions lead to the different fluid temperature distributions. The disturbed TBL patterns in the HXD equipped with the DVB are also differentiable.

Fig. 10 plots the local Nusselt number distributions on duct walls with various g/H values for the type I DVB, $b/H = 0.15$, $Re = 600$ and the +x flow direction. As shown in the figure, it is observed that the g/H ratios lead to the different local Nusselt number patterns. The peak of the heat transfer region is displayed with red contours, while the poor heat transfer region is illustrated with blue contours. The largest area of the red contours is found when $g/H = 0.05$. This means that the $g/H = 0.05$ provides the strongest TBL disturbance (or strongest impinging flows on the duct walls). At the same time, the poor heat transfer regime at corners of the tested duct is obviously detected in the case of $g/H = 0.05$.

Figs. 11, 12 and 13 show the streamlines in cross-sectional planes, temperature in cross-sectional planes and local Nusselt number, respectively, of the tested duct inserted with various DVB types at $Re = 800$, $b/H = 0.20$ and $g/H = 0.10$. The variations of the DVB types and flow directions lead to different flow topologies and heat transfer characteristics. The different flow topologies effect the different locations of the TBL disturbance. Considering at the Nusselt number contours, the largest red contours are found at the type II and I DVB for both +x and -x directions, respectively.

5.2 Thermal performance evaluations

Figs. 14a, b and c show the plots of the Nu/Nu_0 with the Re for the type I, II and III DVB, respectively. The DVB installation leads to the augmented heat transfer rate in all investigated cases ($Nu/Nu_0 > 1$). The heat transfer rate augments with increasing b/H values and Reynolds number.

For the type I DVB, the Nu/Nu_0 is around 1.02 – 6.12, 1.00 – 9.71, 1.03 – 10.50, 1.14 – 11.44 and 1.32 – 14.06, respectively, for $b = 0.05H$, 0.10H, 0.15H, 0.20H and 0.25H. The -x flow direction provides much more heat transfer rates than that of the +x flow direction for $b = 0.05H - 0.15H$ when considering at $Re = 2000$. The greatest Nusselt number is observed at $g = 0.25H$, 0.25H, 0.05H, 0.05H, 0.05H for the +x flow direction at $g = 0.30H$, 0.25H, 0.15H, 0.25H, 0.15H and at $b = 0.05H$, 0.10H, 0.15H, 0.20H and 0.25H for the -x flow direction, respectively.

For the type II DVB, the heat transfer rate is higher than that of the smooth duct (i.e., 1.00 – 6.60, 1.00 – 9.69, 1.00 – 9.97, 1.17 – 11.58 and 1.40 – 13.93 times higher for $b = 0.05H$, 0.10H, 0.15H, 0.20H and 0.25H, respectively). Considering at $Re = 2000$, the -x flow direction yields the upper heat transfer rate than that of the +x flow direction, except for the

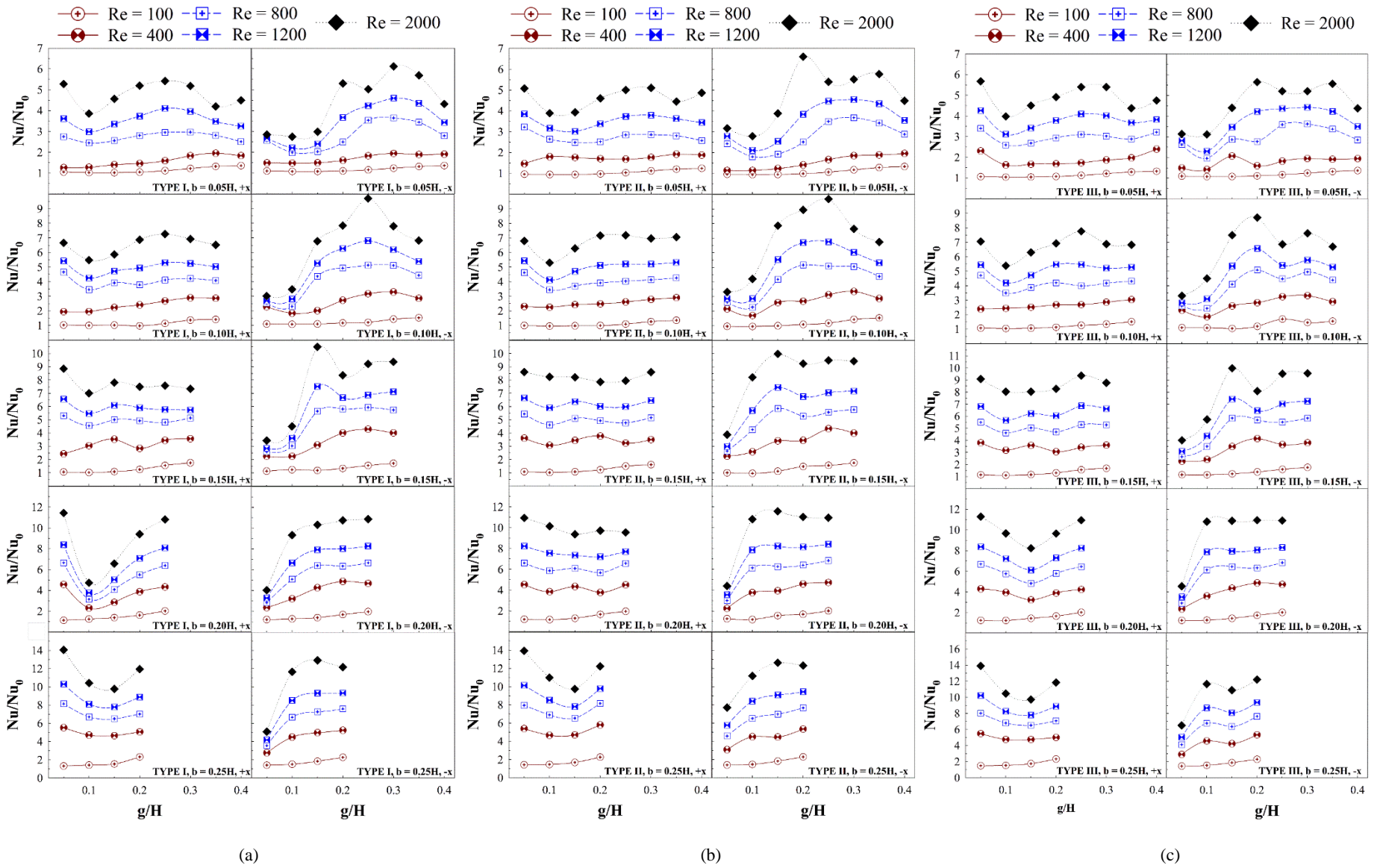


Fig. 14 Nu/Nu₀ vs g/H of the HXD inserted with the DVB for (a) type I, (b) type II and (c) type III.

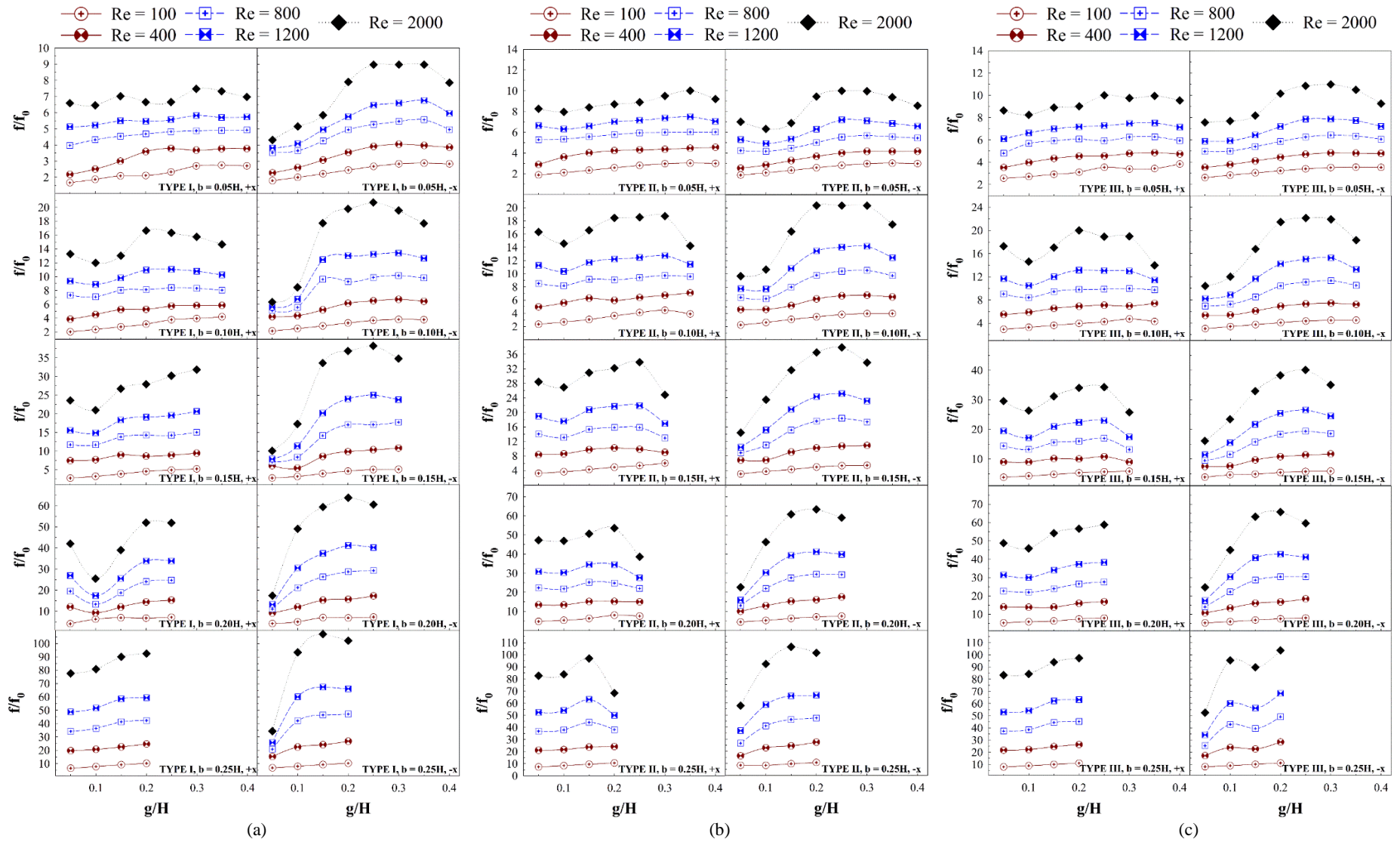


Fig. 15 f/f_0 vs g/H of the HXD inserted with the DVB for (a) type I, (b) type II and (c) type III.

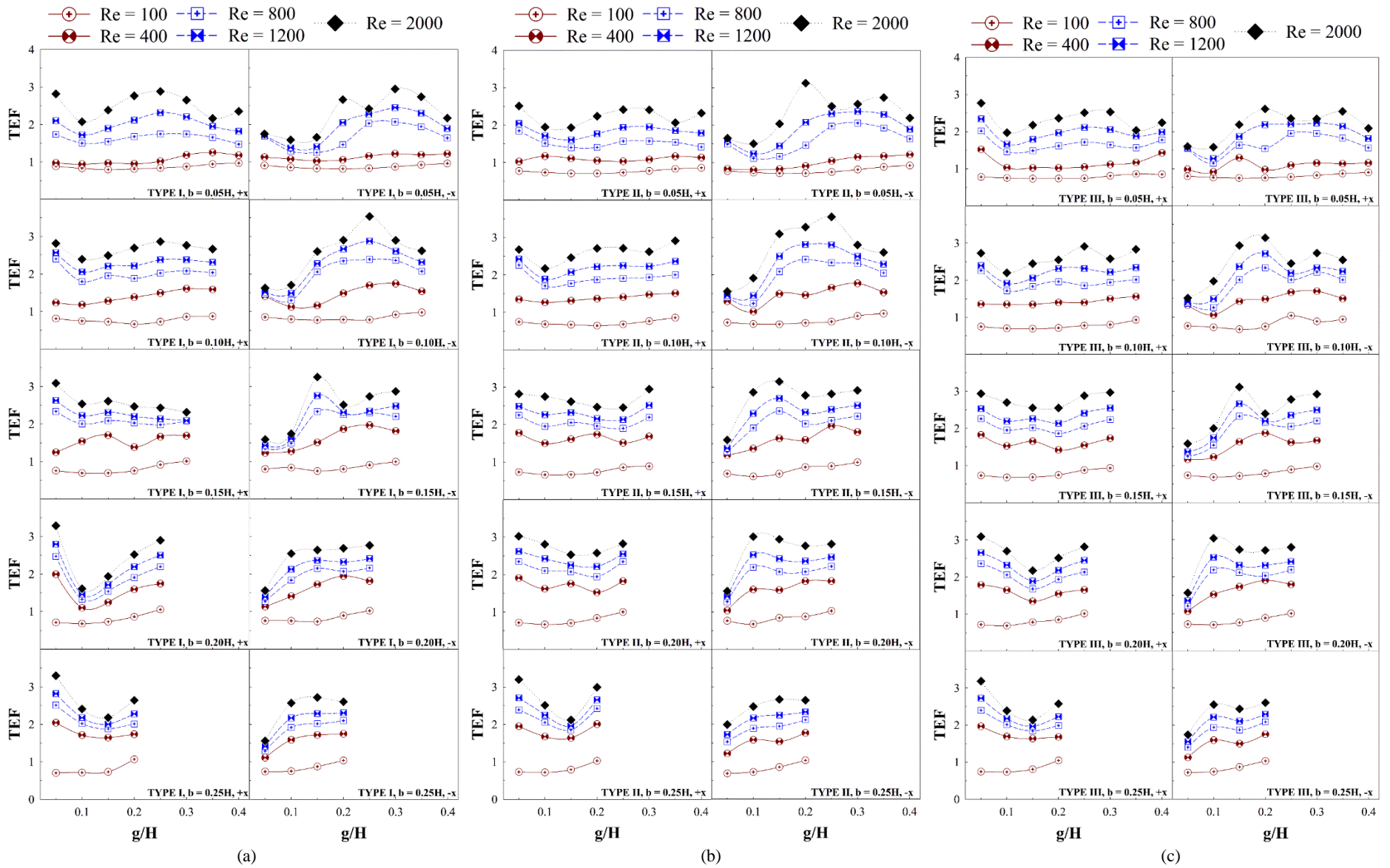


Fig. 16 TEF vs g/H of the HXD inserted with the DVB for (a) type I, (b) type II and (c) type III.

case of $b = 0.25H$. The peak of heat transfer rate is found at $g = 0.30H$, $0.25H$, $0.30H$, $0.05H$, 0.05 for the $+x$ flow direction and at $g = 0.20H$, $0.25H$, $0.15H$, $0.15H$, $0.15H$ for the $-x$ flow direction, respectively, for $b = 0.05H$, $0.10H$, $0.15H$, $0.20H$ and $0.25H$.

For the type III DVB, the heat transfer coefficient is higher than that of the smooth duct with no baffle (i.e., $1.04 - 5.68$, $1.04 - 8.71$, $1.10 - 9.98$, $1.24 - 11.28$ and $1.45 - 13.90$ times higher for $b = 0.05H$, $0.10H$, $0.15H$, $0.20H$ and $0.25H$, respectively). When $Re = 2000$, the highest Nusselt number is obtained at $g = 0.05H$, $0.25H$, $0.25H$, $0.05H$, $0.05H$ for the $+x$ flow direction, at $g = 0.20H$, $0.20H$, $0.15H$, $0.20H$, $0.20H$ for the $-x$ flow direction for $b = 0.05H$, $0.10H$, $0.15H$, $0.20H$ and $0.25H$, respectively.

Figs. 15a, b and c show the plots of the f/f_0 with the Re at different g/H and flow directions for the type I, II and III DVB, respectively. Generally, the f/f_0 increases with an increase in the air velocity and the DVB height.

For the type I DVB, the f/f_0 is $1.67 - 8.98$, $2.04 - 20.70$, $2.77 - 38.27$, $4.09 - 63.86$ and $6.52 - 107.09$, respectively, for $b = 0.05H$, $0.10H$, $0.15H$, $0.20H$ and $0.25H$. The friction loss of the tested duct with the type II DVB is higher than that of the smooth duct with no baffle (i.e., $1.87 - 10.01$, $2.28 - 20.37$, $3.04 - 37.89$, $4.49 - 63.40$ and $7.37 - 106.28$ times higher for $b = 0.05H$, $0.10H$, $0.15H$, $0.20H$ and $0.25H$, respectively). Considering at the type III DVB, the friction factor in the tested duct is much more than the smooth duct (i.e., $2.56 - 10.00$, $2.94 - 22.13$, $3.80 - 40.09$, $5.28 - 65.76$ and $7.93 - 103.64$ times higher for $b = 0.05H$, $0.10H$, $0.15H$, $0.20H$ and $0.25H$, respectively). The peak of the friction factor is found in the range of $g/H = 0.15 - 0.35$ which is subject to the baffle type, the b/H ratio and the flow directions.

Figs. 16a, b and c illustrate the relation of the TEF with the Reynolds number at different g/H and flow directions for the type I, II and III DVB, respectively. In almost cases, the addition of the DVB in the duct results in higher TEF than the plain duct ($TEF > 1$).

For the type I DVB, the best TEF is observed to be 2.88 , 2.86 , 3.09 , 3.29 , 3.30 for the $+x$ flow direction and 2.95 , 3.53 , 3.25 , 2.77 , 2.72 for the $-x$ flow direction, respectively, for $b = 0.05H$, $0.10H$, $0.15H$, $0.20H$ and $0.25H$ at $Re = 2000$. The optimum TEF is at $g/H = 0.25$, 0.25 , 0.05 , 0.05 , 0.05 for the $+x$ flow direction and at $g/H = 0.30$, 0.25 , 0.15 , 0.25 , 0.15 for the $-x$ flow direction for $b/H = 0.05$, 0.10 , 0.15 , 0.20 and 0.25 , respectively.

For the type II DVB, the greatest TEF is found to be 2.51 , 2.91 , 2.95 , 3.02 , 3.20 for the $+x$ flow direction and 3.12 , 3.55 , 3.15 , 3.01 , 2.66 for the $-x$ flow direction, respectively, for $b/H = 0.05$, 0.10 , 0.15 , 0.20 and 0.25 . The best TEF is obtained at $g/H = 0.05$, 0.35 , 0.30 , 0.05 , 0.05 for the $+x$ flow direction and at $g/H = 0.20$, 0.25 , 0.15 , 0.10 , 0.15 for the $-x$ flow direction, respectively, at $b/H = 0.05$, 0.10 , 0.15 , 0.20 and 0.25 .

For the type III DVB, the best TEF is 2.77 , 2.91 , 2.97 , 3.09 , 3.18 for the $+x$ flow direction and 2.61 , 3.13 , 3.11 , 3.04 , 2.60 for the $-x$ flow direction, respectively, for $b/H = 0.05$, 0.10 , 0.15 , 0.20 and 0.25 at $Re = 2000$. The best TEF is observed at $g/H = 0.05$, 0.25 , 0.30 , 0.05 , 0.05 for the $+x$ flow direction and at $g/H = 0.20$, 0.20 , 0.15 , 0.10 and 0.20 for the $-x$ flow direction, respectively, at $b/H = 0.05$, 0.10 , 0.15 , 0.20 and 0.25 . The optimal TEF within the investigated range is tabulated in Table 2 and is shown in Fig. 17.

Table 2. The best TEF of the HXD inserted with the DVB.

| TYPE | b/H | g/H | Flow direction | TEF |
|------|------|------|----------------|-------------|
| I | 0.25 | 0.05 | +x | 3.30 |
| | 0.10 | 0.25 | -x | 3.53 |
| II | 0.25 | 0.05 | +x | 3.20 |
| | 0.10 | 0.25 | -x | 3.55 |
| III | 0.25 | 0.05 | +x | 3.18 |
| | 0.10 | 0.20 | -x | 3.13 |

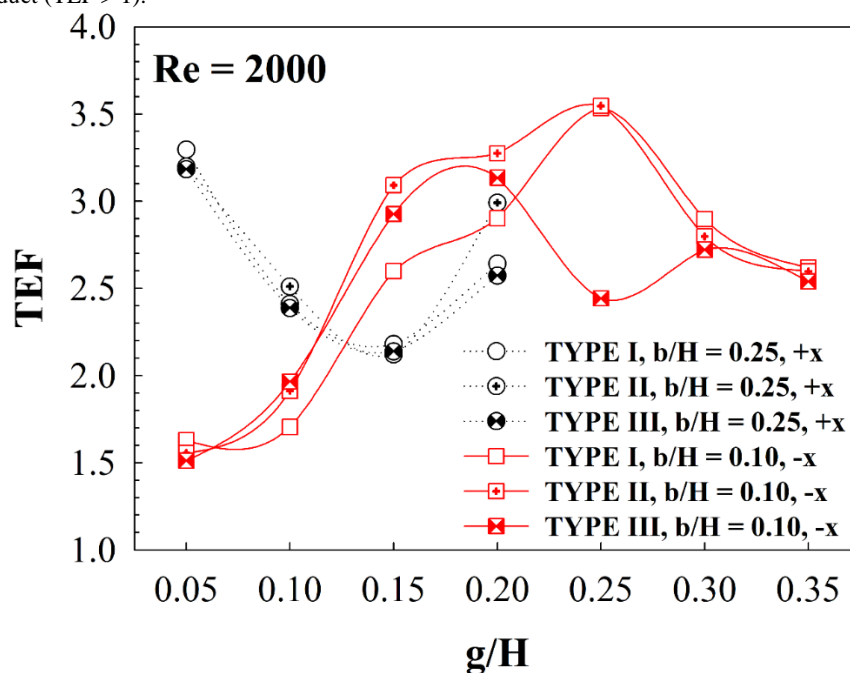


Fig. 17 TEF vs g/H for various DVB configurations, g/H and flow directions at $Re = 2000$.

6. CONCLUSION

Simulations of flow and heat transfer characteristics in the HXD equipped with different configurations of the DVB are performed. The effects of DVB heights ($b/H = 0.05 - 0.25$), baffle locations in transverse plane ($g/H = 0.05 - 0.40$), flow directions ($+x$ and $-x$) and DVB configurations (type I, II and III) on heat transfer and flow patterns are investigated. The HXD performance (Nusselt number, friction factor and TEF) is analyzed. The major findings can be summarized as follows.

The DVB installation leads to greater heat transfer coefficient due to three mechanisms: 1. the generation of the vortex flows through the tested duct, 2. the TBL disturbance and 3. the more efficient fluid mixing. The part of the vortex flows near the duct walls disturbs the TBL, while the other part of the vortex flows at the duct core improves the fluid mixing.

The different flow topologies and heat transfer characteristics in the tested duct are observed with the variation of the g/H ratio, the b/H ratio, flow directions and baffle types. The highest heat transfer rate of the

HXD equipped with the type I, II and III DVB is 14.06, 13.93 and 13.90 times higher than the smooth duct, respectively, at $g/H = 0.05$, $b/H = 0.25$ for the +x flow direction at $Re = 2000$. When considering TEF, the best condition of all DVB types is found at $b/H = 0.25$ and $g/H = 0.05$ for the +x flow direction and at $b/H = 0.10$ and $g/H = 0.20 - 0.25$ for the -x flow direction. The optimum TEF is around 3.55 at $b/H = 0.10$, $g/H = 0.25$ for the -x flow direction at $Re = 2000$.

The DVB has a much higher stabilized structure as compared to previously proposed baffles (Boonloi and Jedsadaratanachai (2020)). In addition, the new DVB structure eases installation in real systems. Our future work will focus on the structure improvement of the vortex generator together with the increments of the vortex strength and turbulent mixing. The study will support a wider range of engineering applications in industries.

ACKNOWLEDGEMENT

The authors would like to thank Assoc. Prof. Dr. Pongjet Promvonge for suggestions.

NOMENCLATURE

| | |
|---------------------|---|
| b | DVB height, m |
| D_h | hydraulic diameter of the duct (=H), m |
| f | friction factor |
| g | gap spacing, m |
| H | square duct height, m |
| h | convective heat transfer coefficient, $W m^{-2} K^{-1}$ |
| k | thermal conductivity, $W m^{-1} K^{-1}$ |
| L | numerical model length/periodic length |
| Nu | Nusselt number ($=hD_h/k$) |
| p | static pressure, Pa |
| P | pitch distance, m |
| Re | Reynolds number |
| T | temperature, K |
| \bar{u} | mean velocity in channel, $m s^{-1}$ |
| W | duct width (=H), m |
| Greek letter | |
| TEF | thermal enhancement factor ($=(Nu/Nu_0)/(f/f_0)^{1/3}$) |
| ρ | density, $kg m^{-3}$ |
| Subscript | |
| 0 | smooth duct |
| pp | pumping power |

REFERENCES

Azad, R., Bhuvad, S., and Lanjewar, A., 2021, "Study of Solar Air Heater with Discrete Arc Ribs Geometry: Experimental and Numerical Approach", *International Journal of Thermal Sciences*, **167**, Article 107013.
<https://doi.org/10.1016/j.ijthermalsci.2021.107013>

Bhuvad, S.S., Azad, R., and Lanjewar, A., 2021, "Thermal Performance Analysis of Apex-up Discrete Arc Ribs Solar Air Heater-an Experimental Study", *Renewable Energy*, **185**, Pages 403-415.
<https://doi.org/10.1016/j.renene.2021.12.037>

Boonloi, A., and Jedsadaratanachai, W., 2020, "Laminar Forced Convection and Performance Evaluation in a Square Duct Heat Exchanger Placed with Wavy Thin Rib", *Frontiers in Heat and Mass Transfer*, 15.1.
<http://dx.doi.org/10.5098/hmt.15.13>

Boonloi, A., and Jedsadaratanachai, W., 2021a, "Impacts of Double V-Rings in the Heat Exchanger Duct on Heat Transfer and Flow Behaviors: A Numerical Study", *Mathematical Problems in Engineering Volume*, Article 1102297.

<https://doi.org/10.1155/2021/1102297>

Boonloi, A., and Jedsadaratanachai, W., 2021b, "Thermal Performance Assessment in a Circular Tube Fitted with Various Sizes of Modified V-baffle: A Numerical Investigation", *Frontiers in Heat and Mass Transfer* 16.
<http://dx.doi.org/10.5098/hmt.16.17>

Cengel, Y.A., and Ghajar, A.J., 2015, "Heat and Mass Transfer: Fundamentals & applications", Fifth edition in SI Units, McGraw-Hill Education, ISBN 978-981-4595-27-8.

Chang, S.W., Chen, T.W., and Chen, Y.W., 2019, "Detailed Heat Transfer and Friction Factor Measurements for Square Channel Enhanced by Plate Insert with Inclined Baffles and Perforated Slots", *Applied Thermal Engineering*, **159**, Article 113856.
<https://doi.org/10.1016/j.applthermaleng.2019.113856>

Chang, S.W., Wu, P.S., and Liu, J.H., 2021, "Aerothermal Performance of Square Duct Enhanced by Twisted Tape with Inclined Ribs and Slots", *International Journal of Heat and Mass Transfer*, **177**, Article 121547.
<https://doi.org/10.1016/j.ijheatmasstransfer.2021.121547>

Du, J., and Hong, Y., 2021, "Numerical Simulation on Fluid Flow and Heat Transfer Characteristics in Inward Sinusoidal Rib Enhanced Tube Heat Exchangers for Waste Heat Recovery: Comparisons and Parametric Studies", *International Journal of Thermal Sciences*, **167**, Article 107030.
<https://doi.org/10.1016/j.ijthermalsci.2021.107030>

Faujdar, S., and Agrawal, M., 2021, "Computational Fluid Dynamics Based Numerical Study to Determine the Performance of Triangular Solar Air Heater Duct Having Perforated Baffles in V-down Pattern Mounted Underneath Absorber Plate", *Solar Energy*, **228**, Pages 235-252.
<https://doi.org/10.1016/j.solener.2021.09.006>

Gill, R.S., Hans, V.S., and Singh, R.P., 2021, "Optimization of Artificial Roughness Parameters in a Solar Air Heater Duct Roughened with Hybrid Ribs", *Applied Thermal Engineering*, **191**, Article 116871.
<https://doi.org/10.1016/j.applthermaleng.2021.116871>

Habet, M.A.E, Ahmed, S.A., and Saleh, M.A., 2021, "Thermal Hydraulic Characteristics of a Rectangular Channel with Inline/staggered Perforated Baffles", *International Communications in Heat and Mass Transfer*, **128**, Article 105591.
<https://doi.org/10.1016/j.icheatmasstransfer.2021.105591> [Get rights and content](#)

Jedsadaratanachai, W., and Boonloi, A., 2014, "Effects of Blockage Ratio and Pitch Ratio on Thermal Performance in a Square Channel with 30° Double V-baffles", *Case Studies in Thermal Engineering*, **4**, Pages 118-128.
<https://doi.org/10.1016/j.csite.2014.08.002>

Jia, B., Liu, F., Li, X., Qu, A., and Cai, Q., 2021, "Influence on Thermal Performance of Spiral Solar Air Heater with Longitudinal Baffles", *Solar Energy*, **225**, Pages 969-977.
<https://doi.org/10.1016/j.solener.2021.08.004>

Kumar, B.V., Manikandan, G., and Kanna, P.R., 2021, "Enhancement of Heat Transfer in SAH with Polygonal and Trapezoidal Shape of the Rib Using CFD", *Energy*, **234**, Article 121154.
<https://doi.org/10.1016/j.energy.2021.121154>

Li, J.L., Tang, H.W., and Yang, Y.T., 2018, "Numerical Simulation and Thermal Performance Optimization of Turbulent Flow in a Channel with Multi V-shaped Baffles", *International Communications in Heat and Mass Transfer*, **92**, Pages 39-50.
<https://doi.org/10.1016/j.icheatmasstransfer.2018.02.004>

Lori, M.S., and Vafai, K., 2022, "Heat Transfer and Fluid Flow Analysis of Microchannel Heat Sinks with Periodic Vertical Porous Ribs", *Applied Thermal Engineering*, **205**, Article 118059.
<https://doi.org/10.1016/j.applthermaleng.2022.118059>

Muñoz-Cámara, J., Crespí-Llorens, D., Solano, J.P., and Vicente, P.G., 2019, "Experimental Analysis of Flow Pattern and Heat Transfer in

Circular-orifice Baffled Tubes", *International Journal of Heat and Mass Transfer*, **147**, Article 118914.
<https://doi.org/10.1016/j.ijheatmasstransfer.2019.118914>

Sahin, B., Ates, I., Manay, E., Bayrakceken, A., and Celik, C., 2019, "Optimization of Design Parameters for Heat Transfer and Friction Factor in a Heat Sink with Hollow Trapezoidal Baffles", *Applied Thermal Engineering*, **154**, Pages 76-86.
<https://doi.org/10.1016/j.applthermaleng.2019.03.056>

Sharma, A., Awasthi, A., Singh, T., Kumar, R., and Chauhan, R., 2022, "Experimental Investigation and Optimization of Potential Parameters of Discrete V down Baffled Solar Thermal Collector Using Hybrid Taguchi-TOPSIS Method", *Applied Thermal Engineering*, Article 118250.
<https://doi.org/10.1016/j.applthermaleng.2022.118250>